# Chapter 2

# Resilient Optimal Gain Control and Continuous Twisting Observer for Enhanced Power System Performance Under Uncertainties

In this chapter of the thesis, resilient optimal gain control is presented for a multimachine power system for mismatched uncertainty compensation and to damp out the inter-area oscillations. The proposed control scheme is analyzed in two sub-steps. In the first step, a power rate reaching law-based virtual control is designed, whereas the main control input in the second step is formulated using optimally tuned gains. Thus, this method does not incorporate multiple differentiation, unlike existing backstepping methods, hence eliminating magnitude limiter, rate limiter & command filter dependency. The controller is designed by separating power system nonlinearities to eliminate complex expression from the control input that reduces the control computation. The proposed method has two steps procedure in control designing that suppresses the recursive step error in multistep virtual control formulation of backstepping methods. Furthermore, a nonlinear observer is designed using continuous twisting law with the integral surface design to counter the mismatched uncertainties along with the disturbance rejection. The proposed scheme is validated in MATLAB/Simulink and in real time digital simulator (RTDS) platform of IEEE standard New England 39-bus, 10-machine power system and compared with the existing methods.

## 2.1 Introduction

The power system is a complex nonlinear system that is built with many other

interconnected subsystems to meet the power demand requirement. Due to power system complexities and mismatches, power system stability is widely affected even under small system perturbations. It is observed that the existing control schemes are focused only on matched uncertainties that exist in the input control channel itself, but the concern of other mismatched uncertainties is left in conventional control schemes for power system networks.

While considering the CF necessity in backstepping control technique, in this chapter of the thesis, a novel control technique is designed that does not incorporate virtual control derivative iterations and hence promotes no CF dependency. The proposed control scheme is designed to be resilient to a fault in the nominal control of a multimachine power system with mismatched uncertainties. A strong fault strength may harshly affect the controller capability and robustness. Although the system stability can be guaranteed through the conventional resilient schemes, the degradation in the system performance may not be evaded. The resilient control applied in this chapter of the thesis is based on the Lyapunov theory, multimachine power system plant, and a closed-loop stabilized control with an equivalent Lyapunov candidate.

Although the backstepping technique is extensively used and well documented in the context of exciting controller design, the complexity of the control scheme is not adequately addressed, which do arise due to derivative term in the successive representation. In this context, the effort is made to initiate a virtual control law independent of the derivative term by virtue of which the control effort is reduced. Any probable occurrence of a fault and sensor nonlinearities may affect controller performance. In lieu of the above resilient controller, a design is made that guarantees stability. Further, the possible manifestation of matched-mismatched uncertainty that arises is also taken into account & an efficient control law is made by continuous twisting control law. It is worthy to mention that the classical backstepping control is accomplished by multiple equations whereas in our control design, derivative terms are reduced to a two-step equation. With these research gaps, optimally tuned resilient control is proposed with the following merits:

- In the proposed control scheme, the control input is obtained by optimally tuned gains with a single virtual iteration. It does not include consecutive virtual derivatives, thus minimizes recursive step error, and promotes no CF [31] as well as higher-order tuner [29] requirements.
- Controller with power rate SMC law is designed by separating power system nonlinear terms, which significantly reduces the control complexity and improves the system performance.
- Continuous twisting nonlinear observer (CTNO) is designed to estimate power system nonlinearity and used to suppress matched/unmatched uncertainties present in the system.
- The resilient control is designed in order to suppress the impact of additive and loss of effectiveness fault in the control signal.

In this scheme, the controller is designed using optimally tuned gains to eliminate CFs and multiple virtual iterations. Further, the observer is designed to estimate system nonlinearities, whereas continuous twisting law is used to extend the robust performance. Resiliency against the loss of effectiveness is proposed, and hence, the overall algorithm provides an additional solidity to damp out the interarea oscillations in the multimachine system.

## 2.2 Power system dynamics & problem formulation

In a multimachine power system interconnected synchronous generators are used to fulfill load demand requirements. Based on projected applications modeling of the multimachine power system can be done in various ways. In multimachine excitation control synchronous generators are extensively represented in 3rd order dynamic model [19], [36], where the $i^{th}$ generator's electrical and mechanical dynamics in an interconnected multimachine power system with $n$ synchronous generators can be represented in 3rd order algebraic/differential equations of the following forms [19], [36]:

$$\dot{\delta} = \omega_i \tag{2.1}$$

And

$$\dot{\omega}_i = -\frac{D_i}{2H_i}\omega_i + \frac{\omega_{0i}}{2H_i}(P_{mi} - P_{ei}) \quad 2.2$$

$$\dot{E}'_{qi} = \frac{1}{T_{doi}}\left(E_{fdi} - E_{qi}\right) \quad 2.3$$

Equation (*2.1*), (*2.2*) and (*2.3*) represents the mechanical and electrical dynamics of $i^{th}$ generator, respectively. From [19] the electrical equations with their usual meaning can be written as:

$$E_{qi} = E'_{qi} - (x_{di} - x'_{di})I_{di} \quad 2.4$$

$$P_{ei} = E'_{qi}I_{qi} \quad 2.5$$

$$Q_{ei} = E'_{qi}I_{di} \quad 2.6$$

$$I_{qi} = \sum_{j=1}^{n} E'_{qj}\left(B_{ij}\,sin\left(\delta_i - \delta_j\right) + G_{ij}\,sin\left(\delta_i - \delta_j\right)\right) \quad 2.7$$

$$I_{di} = \sum_{j=1}^{n} E'_{qj}\left(G_{ij}\,sin\left(\delta_i - \delta_j\right) - B_{ij}\,sin\left(\delta_i - \delta_j\right)\right) \quad 2.8$$

$$V_{ti} = \sqrt{\left(E'_{qi} - x'_{di}I_{di}\right)^2 + \left(x'_{di}I_{qi}\right)^2} \quad 2.9$$

From (*2.1*) to (*2.9*) the dynamic 3rd order synchronous generator in the multimachine power system model can be described as:

$$\dot{\delta} = \omega_i \quad 2.10$$

$$\dot{\omega}_i = -\frac{D_i}{2H_i}\omega_i + \frac{\omega_{0i}}{2H_i}P_{mi} - \frac{\omega_{0i}}{2H_i}E'_{qi}I_{qi} \quad 2.11$$

$$\dot{E}'_{qi} = -\frac{1}{T'_{doi}}E'_{qi} + \frac{(x_{di} - x'_{di})}{T_{doi}}I_{di} + \frac{1}{T_{doi}}E_{fdi} \quad 2.12$$

The dynamics provided in (*2.10*)-(*2.12*) are used to design an excitation control law $E_{fdi}$. This control law will stabilize entire power system states to their equilibrium stability as desired. The control input $E_{fdi}$ will ensure the stability of synchronous generators in the interconnected nonlinear power system networks.

## 2.3 Control problem formulation

Power system networks are intrinsically stable, but the stability is commonly affected by large disturbances such as load variation, critical short-circuit faults, or demand-generation mismatches. In the power system dynamics, the perturbations caused due to load variation may disturb the load current component, and thus the direct current $I_{di}$ is perturbed, whereas the mechanical input power $P_{mi}$ may be perturbed due to variation in the generated and demand power mismatch. Any small perturbation in these parameters wildly affects the system stability in association with the unknown power system parameters (i.e., transient time constants and transient reactance). Therefore, in the proposed scheme, these dynamical power system components as nonlinearity are estimated to mitigate the impact of unknown parameters during perturbations through the formulation of CTNO. Undesirable inter-area oscillations will also appear in the power system network due to the occurrence of external faults.

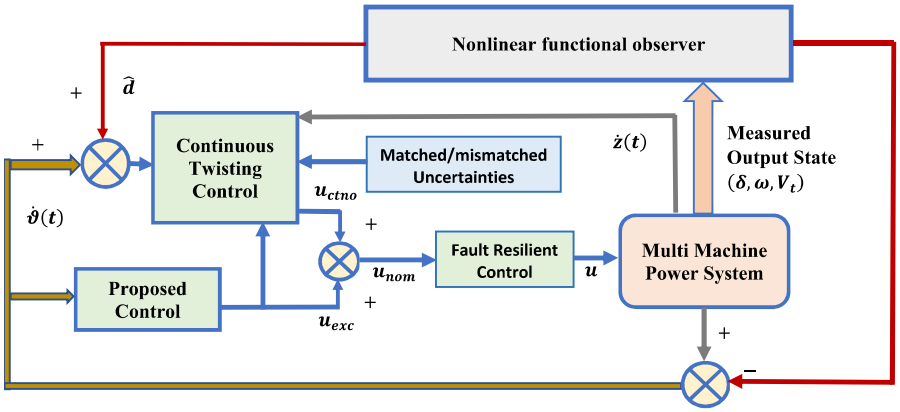


Figure 2.1. Multimachine power system control design.

To overcome such uncertainties along with the disturbances, backstepping control inspired by [37] is proposed for excitation control of multimachine power system using the state dynamical model given in (*2.10*) - (*2.12*), where the control parameters are optimally tuned to achieve the equilibrium power system stability. The main intention is to stabilize the power system states by excitation control under different fault situations along with nonlinear disturbance compensation. Figure *2.1* shows the implementation of overall proposed control scheme. In the figure it is shown that the control $u_{exc}$ is obtained by separating the nonlinearities and the nominal control $u_{nom}$ is achieved by the

combination of $u_{exc}$ and continuous twisting control $u_{ctno}$ , then proposed fault tolerant scheme is applied to $u_{nom}$. Figure *2.1* shows the estimation of nonlinear term $\hat{d}$ which is used to obtained continuous twisting control $u_{nom}$.

Now from the synchronous generator dynamics (*2.10*)-(*2.12*) and nonlinear functional observer (discussed in section 2.3.3), the synchronous generator dynamics for excitation control shown in Figure *2.1* are obtained as:

$$\begin{bmatrix}\dot{x}_1\\ \dot{x}_2\end{bmatrix} = \begin{bmatrix}0 & 1\\ 0 & A_0\end{bmatrix}\begin{bmatrix}x_1\\ x_2\end{bmatrix} + \begin{bmatrix}0\\ A_1\end{bmatrix} y + \begin{bmatrix}0\\ d_1\end{bmatrix} \quad 2.13$$

$$\dot{\mathrm{y}} = A_3\mathrm{y} + A_4 u + d_2 \quad 2.14$$

where $x_1, x_2$ and $y$ are representing $\delta_i, \omega_i$ and $E'_{qi}$ respectively.

$A_0 = -\frac{D_i}{2H_i}, A_1 = -\frac{\omega_{0i}}{2H_i} I_{qi}, A_2 = \frac{\omega_{0i}}{2H_i}, A_3 = -\frac{1}{T'_{doi}}, A_4 = \frac{1}{T_{doi}}$ and $A_5 = \frac{(x_{di} - x'_{di})}{T_{doi}}$. Here $d_1 = A_2 P_{mi}$ and $d_2 = A_5 I_{di}$ are taken as nonlinearities of the power system. Now from the synchronous generator dynamics (*2.10*)-(*2.12*) and nonlinear functional observer (discussed in section 2.3.3), synchronous generator dynamics for excitation control shown in Figure *2.1* are obtained as:

$$\begin{bmatrix}\dot{x}_1\\ \dot{x}_2\end{bmatrix} = \begin{bmatrix}0 & 1\\ 0 & A_0\end{bmatrix}\begin{bmatrix}x_1\\ x_2\end{bmatrix} + \begin{bmatrix}0\\ A_1\end{bmatrix} y \quad 2.15$$

$$\dot{x}_i = Ax_i + Jy \quad 2.16$$

$$\dot{\mathrm{y}} = A_3\mathrm{y} + A_4 u \quad 2.17$$

**Algorithm**

**Control design procedure**

**Step 1:** Select a matrix $\varsigma \in \mathbb{R}^{2\times 2}$ so that the following conditions hold,

$\lambda(A + \varsigma) \in C^{-1}$

$(IA_3 I^{-1} - \varsigma, JA_4)$ is controllable,

$\mathcal{J}_1 \left[A_3\varsigma - \varsigma\left(A + \varsigma \frac{|y|^{1/2}}{\|x_i\|^{1/2}}\right)\right] = 0_{2\times 2}$

where $\mathcal{I}_1 = \begin{bmatrix} 0 & 0 \\ 0 & 1 \end{bmatrix}$.

**Step 2:** Select $\mathcal{M}_1$ as,

$$\mathcal{M}_1 = -\mathcal{I}_2 \left[ A_3 \varsigma - \varsigma \left( A + \varsigma \frac{|y|^{1/2}}{\|x_i\|^{1/2}} \right) \right]$$

With, $\mathcal{I}_2 = \left[ \frac{|y|^{1/2}}{2A_1 A_4 \|x_i\|^{1/2}}, 0 \right]$.

**Step 3:** Finally, set $\mathcal{M}_2$ so that it holds the following inequality.

$$\lambda \left( \frac{1}{2} I A_3 I^{-1} - \varsigma \frac{|y|^{1/2}}{2\|x_i\|^{1/2}} + \frac{JA_4}{2|y|^{1/2}} \mathcal{M}_2 \right) \in C^{-1}$$

**End Procedure**

---

Table 2.1. Algorithm for the proposed control scheme.

### 2.3.1. Design of optimally Tuned Backstepping Excitation Control

In the power system multimachine dynamics as described in (*2.16*)-(*2.17*), further considering $A = \begin{bmatrix} 0 & 1 \\ 0 & A_0 \end{bmatrix}, J = \begin{bmatrix} 0 \\ A_1 \end{bmatrix}$ and $x_i = \begin{bmatrix} x_1 \\ x_2 \end{bmatrix}$ and $JA_4 = \begin{bmatrix} 0 \\ A_1 A_4 \end{bmatrix}$. The excitation control $u$ with the power rate law can be written as:

$$u_{exc} = \mathcal{M}_1 x_i + \mathcal{M}_2 \left( J|y|^{1/2} sign(y) - \varsigma \|x_i\|^{1/2} sign(x_i) \right) \quad 2.18$$

where $\mathcal{M}_1 \in \mathbb{R}^{1\times 2}$, $\mathcal{M}_2 \in \mathbb{R}^{1\times 2}$, and $\varsigma \in \mathbb{R}^{2\times 2}$ are the control design parameters so that the closed-loop multimachine power system (*2.16*)-(*2.17*) is asymptotically stable. The objective is not only to stabilize states but to propose a modular design in such a way that the virtual input differentiation is minimized.

*Proposition 1:* consider the system (*2.16*)-(*2.17*) with controller (*2.18*) having control parametric values $\varsigma$, $\mathcal{M}_1$, and $\mathcal{M}_2$ then the equilibrium of closed-loop multimachine power system states is asymptotically stable.

*Proof:* It starts with the assumption of virtual input $\Delta y$ as [37]:

$$\Delta y = J|y|^{1/2} sign(y) - \varsigma \|x_i\|^{1/2} sign(x_i) \quad 2.19$$

Using the virtual input $\Delta y$, the power system multi-machine dynamics (*2.10*)-(*2.12*) can

be modified as:

$$\dot{x}_\iota = \left(A + \varsigma \frac{|y|^{1/2}}{\|x_i\|^{1/2}}\right) x + |y|^{1/2} \Delta y \tag{2.20}$$

$$\Delta \dot{y} = \frac{1}{2\|x_i\|^{1/2}} \left(A_3 \varsigma - \varsigma \left(A + \varsigma \frac{|y|^{1/2}}{\|x_i\|^{1/2}}\right)\right) x + \frac{1}{2} \left(I A_3 I^{-1} - \varsigma \frac{|y|^{1/2}}{\|x_i\|^{1/2}}\right) \Delta y + \frac{1}{2} \frac{J A_4}{|y|^{1/2}} u_{exc} \tag{2.21}$$

Here the $sign(a) = \frac{a}{|a|}$, & $I \in \mathbb{R}^{2\times 2}$. The value of $\varsigma$ is determined by solving the equation.

$$\mathcal{I}_1 \left[A_3 \varsigma - \varsigma \left(A + \varsigma \frac{|y|^{1/2}}{\|x_i\|^{1/2}}\right)\right] = 0_{2\times 2}$$

Here $\mathcal{I}_1 = \begin{bmatrix} 0 & 0 \\ 0 & 1 \end{bmatrix}$.

Now $\mathcal{M}_1 \in \mathbb{R}^{1\times 2}$ can be determined by solving the following equation,

$$\mathcal{M}_1 = -\mathcal{I}_2 \left[A_3 \varsigma - \varsigma \left(A + \varsigma \frac{|y|^{1/2}}{\|x_i\|^{1/2}}\right)\right]$$

Here $\mathcal{I}_2 = \left[\frac{|y|^{1/2}}{2A_1 A_4 \|x_i\|^{1/2}}, 0\right]$.

$\mathcal{M}_2$ is selected in such a way that the following inequality is satisfied.

$$\lambda \left(\frac{1}{2} I A_3 I^{-1} - \varsigma \frac{|y|^{1/2}}{2\|x_i\|^{1/2}} + \frac{J A_4}{2|y|^{1/2}} \mathcal{M}_2\right) \in C^{-1} \tag{2.22}$$

In (*2.22*) eigen values of R.H.S matrix must have the negative values for the stability of the system. Here $\lambda(.)$ represents the eigen values of the matrix. Now the desired values of $\mathcal{M}_1 and\ \mathcal{M}_2$ can be obtained from the above analysis. By substituting the value of $\mathcal{M}_1$, $\mathcal{M}_2$ and the excitation control law (*2.18*), this control law is placed in (*2.20*) and (*2.21*), yields:

$$\dot{x} = \left(A + \varsigma \frac{|y|^{1/2}}{\|x_i\|^{1/2}}\right) x_i + |y|^{1/2} \Delta y \tag{2.23}$$

$$\Delta \dot{y} = \left(\frac{1}{2} I A_3 I^{-1} - \varsigma \frac{|y|^{1/2}}{2\|x_i\|^{1/2}} + \frac{J A_4}{2|y|^{1/2}} \mathcal{M}_2\right) \Delta y \tag{2.24}$$

The controllability condition implies that there can always be a matrix $\mathcal{M}_2$ exist, so that

(*2.22*) holds. Similarly, there exist symmetric positive definite matrices $P \in \mathbb{R}^{2\times2}$ and $Q \in \mathbb{R}^{2\times2}$ in the proof of proposition 1 in order to satisfy (*2.25*) and (*2.26*) obtained from the optimal stability analysis of a strict positive Lyapunov candidate (*2.27*), $P = P^T > 0$, and $Q = Q^T > 0$,

$$\Upsilon^T Q + Q\Upsilon = -I_{2\times2}, \tag{2.25}$$

$$\left(A + \varsigma\frac{|y|^{1/2}}{\|x_i\|^{1/2}}\right)^T P + P\left(A + \varsigma\frac{|y|^{1/2}}{\|x_i\|^{1/2}}\right) = -I_{2\times2} \tag{2.26}$$

where $\Upsilon = \left(\frac{1}{2}IA_3I^{-1} - \varsigma\frac{|y|^{1/2}}{2\|x_i\|^{1/2}} + \frac{JA_4}{2|y|^{1/2}}\mathcal{M}_2\right)$. Next, let us take a suitably small positive constant $\Im$ and a strict positive Lyapunov candidate (*2.27*) as:

$$\mathcal{L}(x_i, \Delta y) = \Im {x_i}^T P x_i + \Delta y^T Q \Delta y \tag{2.27}$$

Then the time derivative of Lyapunov candidate (*2.27*) along the closed-loop power system trajectories can be written as:

$$\dot{\mathcal{L}}(x_i, \Delta y) = \Im \dot{x_i}^T P x_i + \Im {x_i}^T P \dot{x_i} + \Delta \dot{y}^T Q \Delta y + \Delta y^T Q \Delta \dot{y} \tag{2.28}$$

By putting the values of $\dot{x}$ and $\Delta\dot{y}$ from (*2.20*), (*2.21*) in (*2.28*).

$$\dot{\mathcal{L}}(x_i, \Delta y) = \Im\left({x_i}^T\left(A + \varsigma\frac{|y|^{1/2}}{\|x_i\|^{1/2}}\right)^T + |y|^{1/2}\Delta y^T\right)P x_i + \Im {x_i}^T P\left(\left(A + \varsigma\frac{|y|^{1/2}}{\|x_i\|^{1/2}}\right)x_i + |y|^{1/2}\Delta y\right) + \Delta y^T\left(\frac{1}{2}IA_3I^{-1} - \varsigma\frac{|y|^{1/2}}{2\|x_i\|^{1/2}} + \frac{JA_4}{2|y|^{1/2}}\mathcal{M}_2\right)^T Q\Delta y + \Delta y^T Q\left(\frac{1}{2}IA_3I^{-1} - \varsigma\frac{|y|^{1/2}}{2\|x_i\|^{1/2}} + \frac{JA_4}{2|y|^{1/2}}\mathcal{M}_2\right)\Delta y \tag{2.29}$$

$$\dot{\mathcal{L}}(x_i, \Delta y) = \Im x^T\left[\left(A + \varsigma\frac{|y|^{1/2}}{\|x_i\|^{1/2}}\right)^T P + P\left(A + \varsigma\frac{|y|^{1/2}}{\|x_i\|^{1/2}}\right)\right]x + \Im|y|^{1/2}(\Delta y^T P x_i + x^T P\Delta y) + \Delta y^T\left(\frac{1}{2}IA_3I^{-1} - \varsigma\frac{|y|^{1/2}}{2\|x_i\|^{1/2}} + \frac{JA_4}{2|y|^{1/2}}\mathcal{M}_2\right)^T Q\Delta y + \Delta y^T Q\left(\frac{1}{2}IA_3I^{-1} - \varsigma\frac{|y|^{1/2}}{2\|x_i\|^{1/2}} + \frac{JA_4}{2|y|^{1/2}}\mathcal{M}_2\right)\Delta y \tag{2.30}$$

$$\dot{\mathcal{L}}(x_i, \Delta y) \le \Im x^T\left[\left(A + \varsigma\frac{|y|^{1/2}}{\|x_i\|^{1/2}}\right)^T P + P\left(A + \varsigma\frac{|y|^{1/2}}{\|x_i\|^{1/2}}\right)\right]x + |y|^{1/2}\left(\frac{\Im}{2}{x_i}^T x_i + 2\Im\Delta y^T P^T P\Delta y\right) + \Delta y^T\left(\frac{1}{2}IA_3I^{-1} - \varsigma\frac{|y|^{1/2}}{2\|x_i\|^{1/2}} + \frac{JA_4}{2|y|^{1/2}}\mathcal{M}_2\right)^T Q\Delta y + \Delta y^T Q\left(\frac{1}{2}IA_3I^{-1} - \varsigma\frac{|y|^{1/2}}{2\|x_i\|^{1/2}} + \frac{JA_4}{2|y|^{1/2}}\mathcal{M}_2\right)\Delta y \tag{2.31}$$

Here, $\Delta y^T \Im P x_i + {x_i}^T \Im P \Delta y \leq \frac{\Im}{2} {x_i}^T x_i + 2\Im \Delta y^T P^T P \Delta y$.

From (*2.27*) and the above inequality, it can be written as:

$$\dot{\mathcal{L}}(x_i, \Delta y) \leq -\Im {x_i}^T x_i + \frac{\Im}{2} {x_i}^T x_i + 2\Im \Delta y^T P^T P \Delta y + \Delta y^T \Upsilon^T Q \Delta y + \Delta y^T Q \Upsilon \Delta y \quad 2.32$$

$$\dot{\mathcal{L}}(x_i, \Delta y) \leq -\frac{\Im}{2} {x_i}^T x_i + 2\Im \bar{\tau}_p{}^2 \Delta y^T \Delta y + \Delta y^T (\Upsilon^T Q + Q\Upsilon) \Delta y \quad 2.33$$

$$\dot{\mathcal{L}}(x_i, \Delta y) \leq -\frac{\Im}{2} {x_i}^T x_i - \left(1 - 2\Im \bar{\Xi}_p{}^2\right) \Delta y^T \Delta y \quad 2.34$$

By placing (*2.25*) in (*2.33*), equation (*2.34*) is obtained. Here $\bar{\Xi}_p{}^2 = Max\big(svd(P)\big)$, and $0 < \Im < 1/2\bar{\Xi}_p{}^2$. Hence $\dot{\mathcal{L}}(x_i, \Delta y) \leq 0$, that satisfies the Lyapunov-based stability criteria for the multimachine power system (*2.16*), (*2.17*). It ensures the stability of generator states in power system operation using control (*2.18*). In this chapter of the thesis we have applied the proposed scheme using third order multimachine generator model, it can also be implemented for sixth order detailed model [31] by analyzing the following expression with respect to proposed scheme as provided in (*2.13*), (*2.14*).

$$\begin{bmatrix} \dot{x}_1 \\ \dot{x}_2 \\ \dot{x}_3 \\ \dot{x}_4 \end{bmatrix} = \begin{bmatrix} 0 & 1 & 0 & 0 \\ 0 & A_0 & A_1 & A_2 \\ 0 & 0 & A_3 & 0 \\ 0 & 0 & 0 & A_4 \end{bmatrix} \begin{bmatrix} x_1 \\ x_2 \\ x_3 \\ x_4 \end{bmatrix} + \begin{bmatrix} 0 \\ 0 \\ -A_2 \\ 0 \end{bmatrix} [y] + \begin{bmatrix} 0 & 0 & 0 \\ -A_1 & 0 & 0 \\ 0 & -A_6 & 0 \\ 0 & 0 & A_7 \end{bmatrix} d_1 \quad 2.35$$

$$\dot{\mathrm{y}} = f(\mathrm{y}) + A_5 u + A_5 d_2 \quad 2.36$$

where $A_0 = -\frac{D_i}{2H_i}$, $A_1 = -\frac{\omega_{0i}}{2H_i} I_{qi}$, $A_2 = \frac{\omega_{0i}}{2H_i} I_{di}$, $A_3 = -\frac{1}{T'_{doi}}$, $A_4 = -\frac{1}{T'_{qoi}}$, $A_5 = \frac{K_{Ai}}{T_{Ai}}$, $A_6 = \frac{(x_{di} - x'_{di})}{T_{doi}}$, $A_7 = \frac{(x_{qi} - x'_{qi})}{T_{qoi}}$, $d_1 = [P_m \quad I_{di} \quad I_{qi}]^T$, and $d_2 = \left(V_{refi} - V_{ti}\right)$.The system states can be taken as $x_1 = \delta_i$, $x_2 = \omega_i - \omega_{0i}$, $x_3 = E'_{qi}$, $x_4 = E'_{di}$, $\mathrm{y} = E_{fdi}$, and control input $u = V_{ci}$.

### 2.3.2. Design of Nonlinear functional Observer and Continuous Twisting control

A robust nonlinear observer is required to estimate power system nonlinearities as per Figure *2.2*. The Figure *2.2* explain the estimation of $\hat{d}_k$, which is used to design continuous twisting control law (*2.50*), that is further added to the excitation control input (*2.18*).

Also the designing process of the nonlinear observer is explained in Figure *2.2*. To design the nonlinear observer first, the synchronous generator dynamics of the multimachine power system are given in (*2.10*)-(*2.12*) and can be written in the following form.

$$\dot{z} = f_1(z) + g(z)u_{nom} + \sum_{k=1}^{2} h_k d_k \tag{2.37}$$

with,

$$f_1(z) = \begin{bmatrix} x_2 \\ -\frac{D_i}{2H_i}x_2 - \frac{\omega_{0i}I_{qi}}{2H_i}\mathrm{y} \\ -\frac{\mathrm{y}}{T'_{doi}} \end{bmatrix}, g(z) = [0 \quad 0 \quad A_4]^T, h_1 = [0 \quad A_2 \quad 0]^T$$

and $h_2 = [0 \quad 0 \quad A_5]^T$.

### 2.3.3. Nonlinearity estimation with the nonlinear Observer.

The nonlinear observer is designed to estimate the nonlinearity $d_i$, as:

$$\hat{d}_k = \eta_k + p_k(z) \tag{2.38}$$

$$\dot{\eta}_k = -\ell(z)h_k\,\eta_k - \ell(z)(h_k p_k(z) + f_1(z) + g(z)u_{nom}) \tag{2.39}$$

where $k = 1,2$. The $\hat{d}_k$ is the estimate of nonlinearity and $\eta_k$ is a nonlinear observer's internal state, respectively. A nonlinear function $p_k(z)$ is designed parameter that is described as:

$$p_k(z) = \ell_1 x_1 + \ell_2 x_2 + \ell_3 y$$

The gain of this nonlinear observer $\ell(x)$ is described as:

$$\ell(z) = \frac{\partial p_k(z)}{\partial(z)}$$

*Assumption 1:* The nonlinearity $\hat{d}_k$ in the generator dynamics (*2.13*), (*2.14*) satisfies the following condition:

$$\begin{cases} d_k{}^* = \sup\limits_{t>0} |d_k(t)| \\ \lim\limits_{t\to\infty} \dfrac{d d_k(t)}{dt} = 0 \end{cases} \tag{2.40}$$

It should be noted that the nonlinearity $\hat{d}_k$ in the multimachine power system satisfied the above assumption. Equation of error convergence can be derived from the assumption in (*2.40*), as:

$$\frac{de_{d_k}(t)}{dt} + (\ell(z)h_k)e_{d_k}(t) = 0 \qquad 2.41$$

Here, $e_{d_k}(t) = d_k(t) - \hat{d}_k(t)$.

Now (*2.41*) is asymptotically stable. Therefore,

$$\lim_{t\to\infty} e_{d_k}(t) = 0 \qquad 2.42$$

If the nonlinear observer gains $\ell(z)$ is chosen such that $\ell(z)h_k > 0$, that ensures (*2.42*) will be globally asymptotically stable [27], nonlinearity estimation $\hat{d}_k(t)$ of the nonlinear observer in (*2.38*), (*2.39*) can achieve the nonlinearity $d_k(t)$ of the generator dynamics (*2.37*) asymptotically with $\frac{1}{\ell(z)h_k}$ time constant.

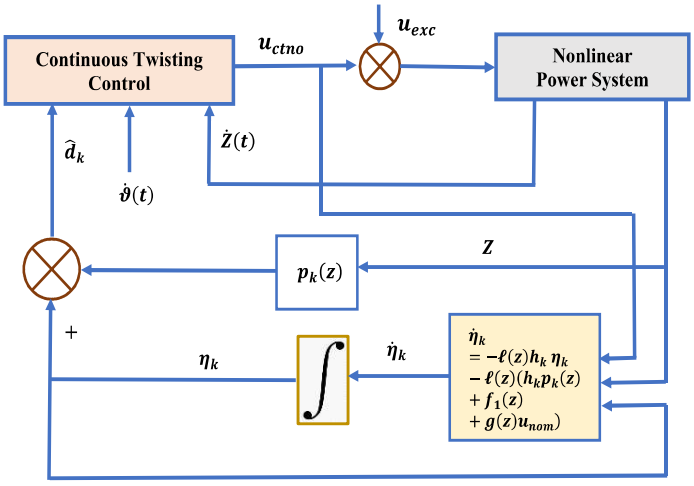


Figure 2.2 Nonlinearity observer block.

Figure 2.2 shows overall structure of the proposed observer. Here the feedback signals are obtained from the generator and processed to obtain $\dot{\eta}_k$ from (2.39). An integrator is used to achieve value of $\eta_k$. The signal $p_k(z)$ is obtained from the feedback signal. By adding these signal $\eta_k$ and $p_k(z)$ the nonlinear term $\hat{d}_k$ is obtained as per equation (2.38).

### 2.3.4. Continuous twisting algorithm for matched/mismatched uncertainties in the presence of power system nonlinearities.

Matched/mismatched uncertainty can be expressed as [28].

$$\wp(e) = \wp_m(e) + \wp_{mm}(e) \qquad 2.43$$

where $\wp_m(e)$ & $\wp_{um}(e)$ are the matched & mismatched uncertainties expressed as

$\wp_m(e) = gg^{\aleph}\wp(e)$ and $\wp_{mm}(e) = g^{\urcorner}(g^{\urcorner})^{\aleph}\wp(e)$ with $g^{\aleph} = [g^T g]^{-1}g^T$. The $g^{\urcorner}$ can be obtained from, ${g^{\urcorner}}^T g = 0$. Here $g^{\urcorner} = [1 \quad 0 \quad 0]^T$.

In this section, an integral sliding mode (ISM) is used for compensation of matched/mismatched uncertainties and disturbance rejection in the presence of power system nonlinearities using continuous twisting reaching law [38]. Here the integral sliding surface is selected using nonlinear estimation of (*2.38*), (*2.39*). In (*2.43*) $G$ is the projection matrix. This is calculated in such a way that, $[G(g)]^{-1}$ will be nonsingular. The integral sliding surface is designed [39] with integral term is used in (*2.44*) to decay the disturbances exponentially as:

$$s(t) = G\left[z(t) - \int_0^t \dot{\vartheta}_1(\tau)d\tau\right] \tag{2.44}$$

Here, $G$ is a parameter designed such that $Gh_k$ is invertible. The function $\dot{\vartheta}_1(\tau)$ is defined as:

$$\dot{\vartheta}_1(\tau) = \dot{\vartheta}(\tau) + \sum_{k=1}^{2} h_k \hat{d}_k \tag{2.45}$$

where $\dot{\vartheta}(\tau) = f(z) + g(z)u_{exc}$ as given in (*2.10*)-(*2.12*). Now, taking the first derivative of integral sliding surface $s(t)$ in (1.44) is written as:

$$\dot{s}(t) = G\left[\dot{z}(t) - \dot{\vartheta}_1(\tau)\right]$$

By using (*2.37*) and (*2.45*), also $u_{nom} = u_{exc} + u_{ctno}$, here the $u_{ctno}$ is the CTNO control input.

$$\dot{s}(t) = G\left[gu_{ctno} + \sum_{k=1}^{2} h_k e_{d_k}(t) + + gg^{\aleph}\wp(e) + g^{\urcorner}(g^{\urcorner})^{\aleph}\wp(e)\right] \tag{2.46}$$

Next, the second derivative of the integral sliding surface can be written as:

$$\ddot{s}(t) = G\left[g\dot{u}_{ctno} + \sum_{k=1}^{2} h_k \dot{e}_{d_k}(t) + gg^{\aleph}\dot{\wp}(e) + g^{\urcorner}(g^{\urcorner})^{\aleph}\dot{\wp}(e)\right] \tag{2.47}$$

A second order sliding surface with continuous twisting reaching law [38], [39] is written as:

$$\ddot{s}(t) = -k_1|s|^{1/2}sign(s) - k_2|\dot{s}|^{1/3}sign(\dot{s}) + \Im \quad 2.48$$

$$\dot{\Im} = -k_3 sign(s) - k_4 sign(\dot{s}) \quad 2.49$$

Therefore, the control input $u_{ctno}$ can be designed with the assumption (*2.42*) as:

$$u_{ctno} = -(Gg)^{-1}\left[\int_0^t \left(k_1|s|^{1/2}sign(s) + k_2|\dot{s}|^{1/3}sign(\dot{s}) - \Im + G\dot{\wp}_{mm}(e)\right)dt\right] + g^{\aleph}\wp(e) \quad 2.50$$

The input $u_{ctno}$ permits the controller to reject disturbances with bounded derivatives. The sensitivity analysis of continuous twisting and super twisting schemes with respect to disturbance rejection capability is omitted here due to the compactness of the presentation, the detail can be found in [39]. Resilient Control Scheme Further to extend the controller performance for fault resiliency through nominal control $u_{nom}$ is analyzed in this section. The notion here is based on Lyapunov study, in a way that if a Lyapunov candidate-based stabilizing closed-loop controller exists, then a fault resilient controller can be designed depending upon the Lyapunov candidate and nominal control to assure the stability of the system during fault [40].

Specifications and Values of System Parameters

| Quantity | Specification |
|---|---|
| $E_f(pu)$ | 1.90805 |
| $E_{min}(pu)$ | $\pm 5$, |
| $V_T(pu)$ | $1.03\,Volt$ |
| $H$ | $2.43sec$ |
| $x'_d(pu)$ | 0.57 |
| $x_d(pu)$ | 2.9 |
| $T'_{do}$ | $0.003sec$ |
| $T_{do}$ | $6.7sec$ |
| $R_{G8}(pu)$ and $X_{G8}(pu)$ | 0.00686, 0.280 |
| $R_{B25-B26}$ and $X_{B25-B26}$ | 0.0032,0.0323 |
| Proposed controller gains | $k_1 = 1.223, k_2 = 3.23, k_3 = 0.84, k_4 = 2.13$ |
| Controller parameters [38], [24] and [41] | $c_1 = c_2 = c_3 = 2, \gamma = 2, \rho = 4, \alpha = 0.1, \alpha_1 = \beta_1 = \alpha_2 = \beta_2 = \alpha_3 = \beta_3 = \alpha_4 = \beta_4 = 0.2, \tau_1 = \tau_2 = 0.2$ |

Table 2.2. Specifications and Values of System Parameters

The nonlinear synchronous generator dynamics presented in (*2.37*) can be rewritten as:

$$\dot{z} = f_2(z) + g(z)u_{nom} \tag{2.51}$$

where $f_2(z) = \begin{bmatrix} x_2 \\ -\frac{D_i}{2H_i}x_2 - \frac{\omega_{0i}I_{qi}}{2H_i}\mathrm{y} + A_2 \\ -\frac{\mathrm{y}}{T'_{doi}} + A_5 \end{bmatrix}$.

The (*2.52*) satisfies $\|z(t)\| \leq \gamma(\|z(t_0)\|, t - t_0), \forall x_{t_0} \in D$ for all $\forall t \geq t_0$, where, $D = \{x \in \mathbb{R}|_{\|x\|<a_0}\}, a_0 > 0$ and $\gamma$ is a function of $\mathcal{KL}-$class. Any strictly increasing continuous function $\alpha: [0, c) \to [0, c)$ with $\alpha(0) = 0$ belongs to class$-\mathcal{K}$. Similarly, class$-\mathcal{KL}$ for the continuous function is defined as if, for every fixed $l$, the mapping of $\gamma(a, l)$ belongs to class$-\mathcal{K}$ pertaining to $a$, and for every fixed $a$, mapping of $\gamma(a, l)$ decreases pertaining to $l$, and $\gamma(a, l) \to 0$ as $l \to \infty$ [[41]. Page no. 144].

*Assumption 2:* The model (*2.52*) is considered here for the resiliency of power system control $u_{nom}$ as:

$$\dot{z} = f_2(z) + g(z)\big(u_{nom} + \mathcal{F}(t, z)\big) \tag{2.52}$$

where $\mathcal{F}$ denotes the fault $\ni \|\mathcal{F}(t, z)\| \leq \propto (t, z)$ with $\propto$ as a positive continuous function.

*Remarks:*

1) From the power system dynamics described in (*2.51*), which simplifies that the closed-loop power system (*2.10*)-(*2.12*) is uniformly and asymptotically stable in $D$.

2) Assumption 2 is not limiting and therefore satisfies the practical power system application, e.g., additive excitation faults occurring in the field voltage and the loss of effectiveness in the nominal control of excitation field voltage. Now, the resilient control in the multimachine power system scenario can be stated as:

With the stabilizing control (*2.18*), a stabilizing closed-loop control for fault case (*2.52*) is required for the power system resiliency. The control $u$ for the faulty system, as assumed in (*2.52*) can be written as:

$$u(t, x) = u_{nom}(t, x) - sat\left(\left(\frac{\partial \mathcal{L}}{\partial x}g\right)^T\right)(\propto(t, x) + \varepsilon) \tag{2.53}$$

Where, $\varepsilon$ is a positive constant as $\varepsilon > 0$ with $sat(.)$ defined as:

$$sat(s) = \begin{cases} s(i)/\tilde{\epsilon} & |s(i)| \le \tilde{\epsilon} \\ sign(s(i)) & |s(i)| > \tilde{\epsilon} \end{cases}$$

*Proof:* It can be ensured from [[41], Page No. 167, Th. 4.16] a positive Lyapunov candidate $\mathcal{L}: [0\infty) \times D \to \mathbb{R}$ exists such that:

$$\alpha_1(\|x\|) \le \mathcal{L}(t,x) \le \alpha_2(\|x\|) \quad 2.54$$

$$\frac{\partial \mathcal{L}}{\partial t} + \frac{\partial \mathcal{L}}{\partial x}(f_2 + g u_{nom}) \le -\alpha_3(\|x\|) \quad 2.55$$

$$\left\|\frac{\partial \mathcal{L}}{\partial x}\right\| \le \alpha_4(\|x\|) \quad 2.56$$

where $\alpha_i \; with \; i = 1..4$ belongs to $\mathcal{K}$ −class functions in $D$. The derivative of $\mathcal{L}$ along the fault (*2.52*) using control (*2.53*) is written as:

$$\frac{d\mathcal{L}}{dt} = \frac{\partial \mathcal{L}}{\partial x}\left(f_2 + g(u + \mathcal{F})\right) + \frac{\partial \mathcal{L}}{\partial t} \quad 2.57$$

$$\frac{d\mathcal{L}}{dt} = \frac{\partial \mathcal{L}}{\partial x} f_2 + \frac{\partial \mathcal{L}}{\partial x} g u + \frac{\partial \mathcal{L}}{\partial x} g\mathcal{F} + \frac{\partial \mathcal{L}}{\partial t} \quad 2.58$$

$$\frac{d\mathcal{L}}{dt} \le \frac{\partial \mathcal{L}}{\partial t} + \frac{\partial \mathcal{L}}{\partial x} f_2 + \frac{\partial \mathcal{L}}{\partial x} g(u_{nom} + \bar{u}) + \frac{\partial \mathcal{L}}{\partial x} g\mathcal{F}$$

$$\frac{d\mathcal{L}}{dt} \le -\alpha_3(\|x\|) + \frac{\partial \mathcal{L}}{\partial x} g\bar{u} + \frac{\partial \mathcal{L}}{\partial x} g\mathcal{F}$$

where, $\bar{u} = -sgn\left(\left(\frac{\partial \mathcal{L}}{\partial x} g\right)^T\right)(\propto(t,x) + \varepsilon)$

$$\frac{d\mathcal{L}}{dt} \le -\alpha_3(\|x\|) - \left\|\frac{\partial \mathcal{L}}{\partial x} g\right\|(\propto + \varepsilon) + \left\|\frac{\partial \mathcal{L}}{\partial x} g\right\| \propto(t,x)$$

$$\frac{d\mathcal{L}}{dt} \le -\alpha_3(\|x\|) - \left\|\frac{\partial \mathcal{L}}{\partial x} g\right\| \varepsilon$$

$$\frac{d\mathcal{L}}{dt} \le -\alpha_3(\|x\|)$$

The derivative of the Lyapunov function is hence negative as per [[41], page no.151,152, Th.48, Th.49], using control (*2.53*) for the fault case of (*2.52*), $\forall x \in D$ and thus the system is uniformly asymptotic stable [40].

## 2.4 Controller verification and simulation results

Simulation is carried out in MATLAB/Simulink platform. The IEEE 39-bus, 10-machines New England power system model, as shown in Figure *2.3*, is selected for the

controller verification. The system parameter's detail can be found in [16] for evaluation of the proposed control scheme. The power system of the Figure *2.3* model consists of both dynamic & static loads having 6150.5 MW load demand and 6193.41 MW of power generation through the 10 synchronous machine generators. To prevent the problem of overvoltage, $\pm 5\ pu$ limit is considered for all exciter's excitation voltages. Variation in the load is not considered in the simulation. Therefore, the turbine-governor dynamics are omitted. In this chapter of the thesis, the power system nonlinearities as the mechanical power input and the direct current are estimated through nonlinear observer and other recent controllers. Based on modal analysis [16] the generator $G8$ connected at bus-37 is taken to test the controller efficacy instead of applying it to all generators as a cost-effective solution. All system parameters and controller gains are provided in Table 2.2.

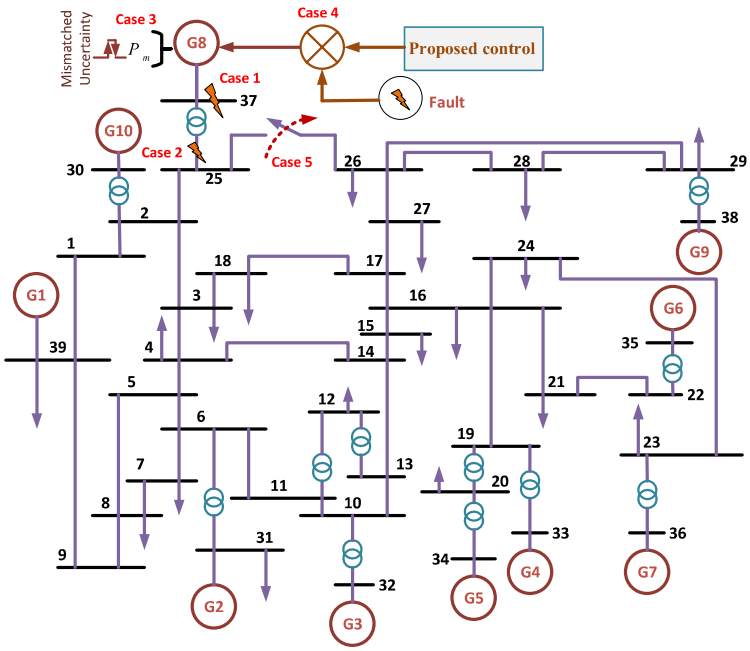


Figure 2.3. IEEE 39 Bus, 10-Machine new England Power System.

*Details of IEEE 10 machine 39 Bus model:* The IEEE 10 machine 39-bus system investigated in this chapter of the thesis, as illustrated in Figure *2.3* is often known as the 39 Bus New-England Power System model. This IEEE 39 bus model of power system used for simulation analysis is a highly symmetrical structure that consists of capacitor banks, loads, generators, and transmission lines. In the 39 bus multimachine model, each

machine or generator is characterized as a voltage source with the source impedance of 10Ω. The corresponding transmission lines and loads are modeled using the Bergeron model and as a constant PQ load, respectively. The two-axis synchronous generator model is taken for all generators in the network. The generator-1 signifies the aggregation of the power system connected to bus number 39, and a constant field voltage and mechanical torque is supplied to it.

To examine the controller performance following five cases are carried out.

- *Case 1:* A three-phase short circuit fault at the terminal of $G8$ is applied for $0.2\ sec$.
- *Case 2:* A three-phase short circuit fault between transmission line bus-25 and bus-37 is applied for $0.2\ sec$.
- *Case 3:* Step perturbation (mismatched uncertainties) in the mechanical power at $G8$ is applied.
- *Case 4:* A loss of effectiveness with constant and periodic faults in the $u_{nom}$ is added at $t = 5\ sec$.
- *Case 5:* Temporary line trip between bus-25 and bus-26 is applied for $0.2\ sec$.

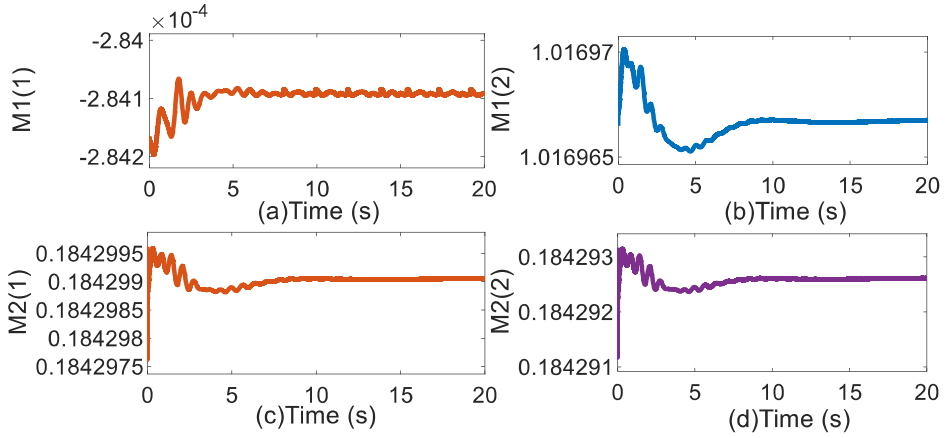


Figure 2.4. Optimal gain parameters response.

In the first two cases, faults are taken as three-phase short circuit fault, which is initiated at $t = 6\ sec$ and clear at $t = 6.2\ sec$. In contrast, the third case is initiated at $t = 5\ sec$ for a duration of $0.2\ sec$. In cases 1 and 2, the proposed controller performance is compared with adaptive backstepping methods given in [24], [42], with the parameters

given in Table 2.2. The response of optimally tuned gains (*2.18*) is illustrated in in Figure *2.4*. To visualize the external disturbance as environmental noise in the form of uncertainties in power system simulation, white Gaussian noises with a 40 $dB$ signal to noise ratio are considered in all simulation cases, as illustrated in Figure *2.5*(a).

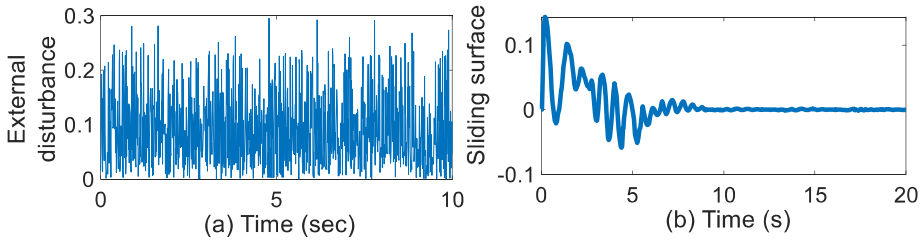


Figure 2.5. (a) White Gaussian noises as an external disturbance. (b) Sliding surface.

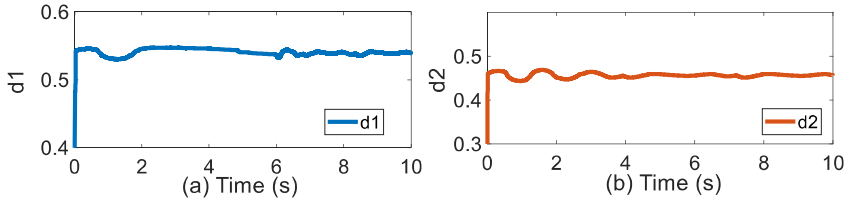


Figure 2.6. Estimation of nonlinearity (a) $d_1$ (b) $d_2$.

In Figure *2.5*(b) the response of the sliding surface as per (*2.44*) is illustrated. Similarly, the power system nonlinearities are estimated through the proposed CTNO as depicted in Figure *2.6*(a) and (b). Where Figure *2.6*(a) is the estimation of $\hat{d}_1$ and Figure *2.6*(b) depicts the estimation of $\hat{d}_2$ per unit.

*Case 1:* In this case, a three-phase short-circuit terminal fault of 0.2 $sec$ is applied at $G8$ from $t = 6\ sec$. The proposed scheme exhibits a fast response with reduced overshoot due to its optimal resiliency and simplified control dynamics. The proposed scheme has a fast-convergent response of the terminal voltage at $G8$ as compared with adaptive backstepping methods [24], [42] and fractional order control [43], as illustrated in Figure *2.7* (a). In backstepping methods [24], [42], and [43], the higher control magnitude is reflected due to complex control expression with higher-order derivative terms. The speed deviation response is oscillatory at the fault occurrence and gradually settles to a pre-fault value after the fault clearance.

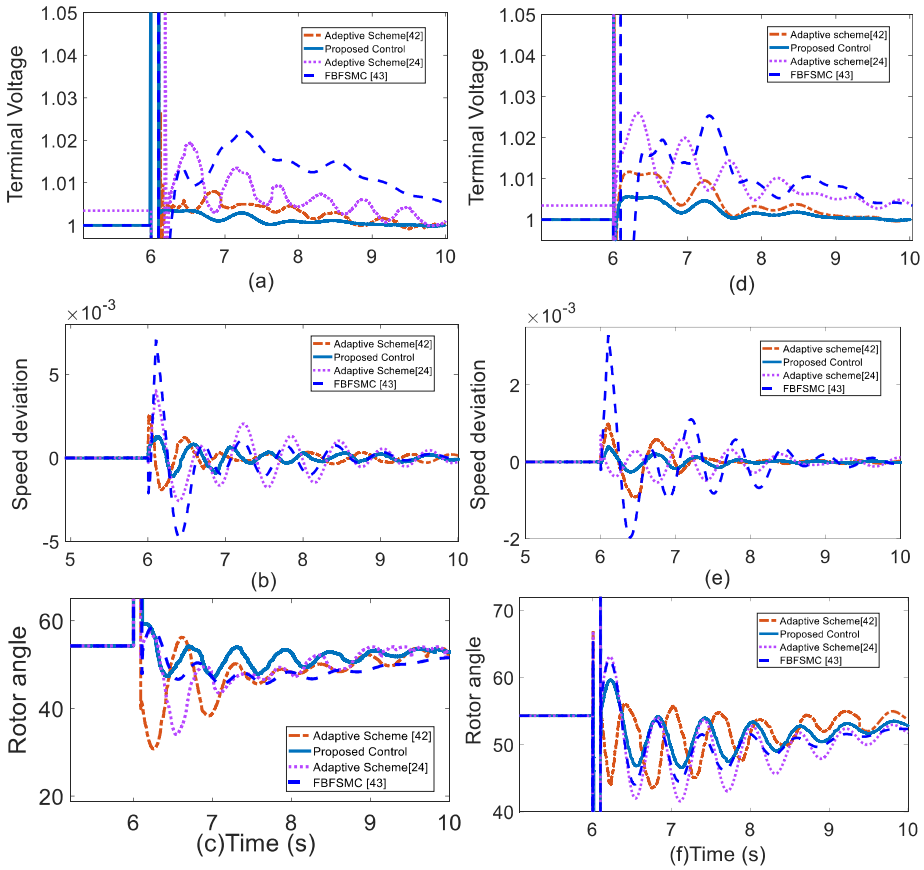


Figure 2.7. Response of proposed control with the adaptive backstepping methods [24], [42], [43] under case 1: (a) terminal voltage $G8$ (b) speed deviation (c) rotor angle. Case 2: (d) terminal voltage $G8$ $(pu)$ (e) speed deviation $(pu)$ (f) rotor angle.

The result in Figure *2.7*(b) shows the fast response of the proposed control action as it provides more damping to the system and exhibits a superior response. A similar control action is obtained in the response of rotor angle as it achieves the pre-fault value after the clearance of the terminal fault faster than the other backstepping schemes. The corresponding control signal for case 1 is illustrated in Figure *2.8*(a). it can be observed from the results in Figure *2.8*(a) that the proposed scheme has applied less effort as compared with the backstepping methods [24], [42], and [43]. In [43] control signal consists of the major complexity with fraction order derivative terms; therefore, it exhibits more control effort. The better efficacy of the proposed control action is obtained due to the reduced nonlinearities in the control structure.

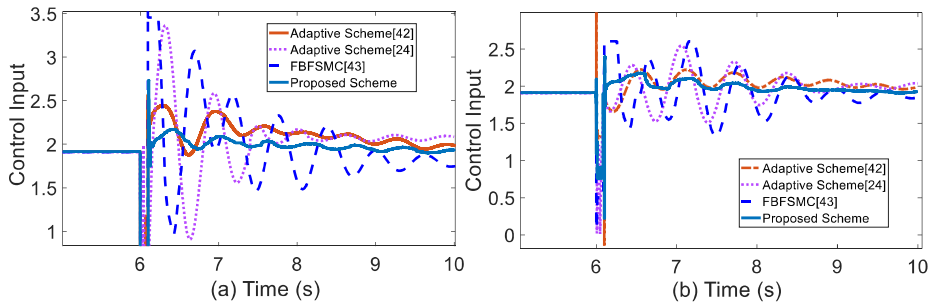


Figure 2.8. Control inputs $(pu)$ of proposed control, and backstepping methods [24],[42] and [43] for (a) case 1 (b) case 2.

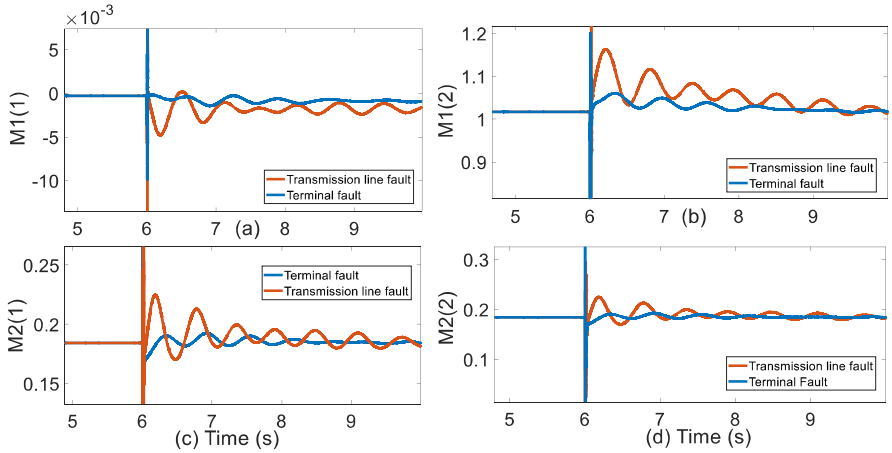


Figure 2.9. Optimal gain parameters (a) M1(1) (b) M1(2) (c) M2(1) (d) M2(2).

*Case 2:* A three-phase short circuit fault is applied at the transmission line between buses 25 and 37. The terminal voltage, speed deviation, and rotor angle responses are shown in Figure *2.7*(d), (e), and (f), respectively. All responses are perturbed at the time of fault, as depicted in the results. Again, the proposed scheme has reflected a faster response with less overshoot as compared to backstepping schemes [24], [42], and [43]. This observation is obtained due to control design simplification and robust action of continuous twisting-based observer. The respective control input for case 2 is shown in Figure *2.8*(b). The control input has shown $0.18$ pu less effort as compared with the adaptive backstepping schemes [24], [42], and $0.2pu$ less effort as compared with the scheme [43]. Optimal gain variation under case-1 & 2 is presented in Figure *2.9*.

### 2.4.1. Controller efficacy under uncertainty.

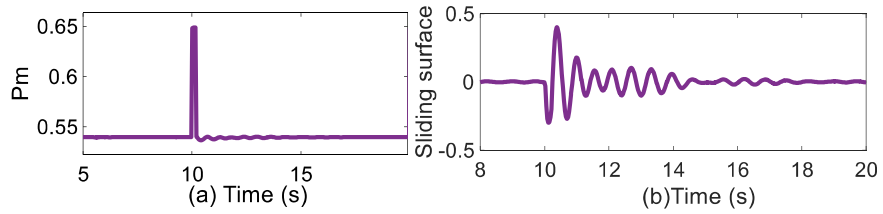


Figure 2.10. Step change in (a) mechanical input power $(pu)$ (b) Sliding surface

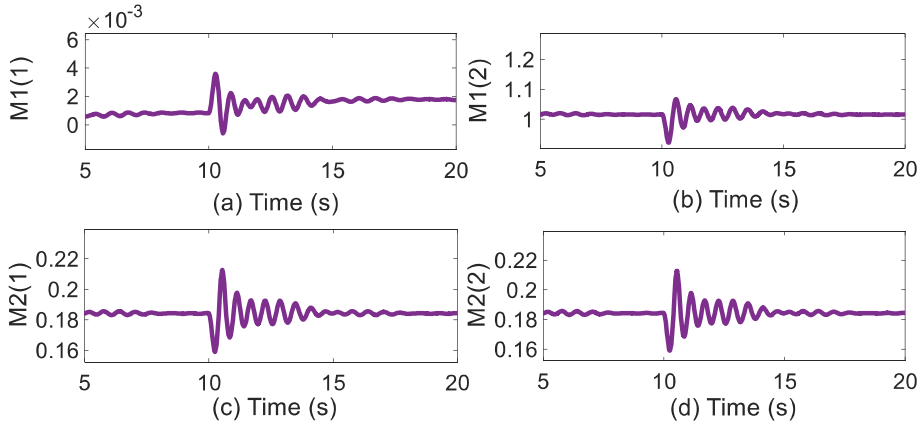


Figure 2.11. Optimal gain parameters (a) M1(1) (b) M1(2) (c) M2(1) (d) M2(2).

*Case 3:* In this case, the mechanical power at $G8$ is perturbed at $t = 10\ sec$ to study the impact of uncertainties in the power system network. The sudden small step change in mechanical input power at $G8$ is shown in Figure *2.10*(a) as uncertainty, and the corresponding change in sliding surface is depicted in Figure *2.10*(b). This small perturbation in the mechanical input power is considered to analyze the impact of dynamical nonlinearities on the control performance.

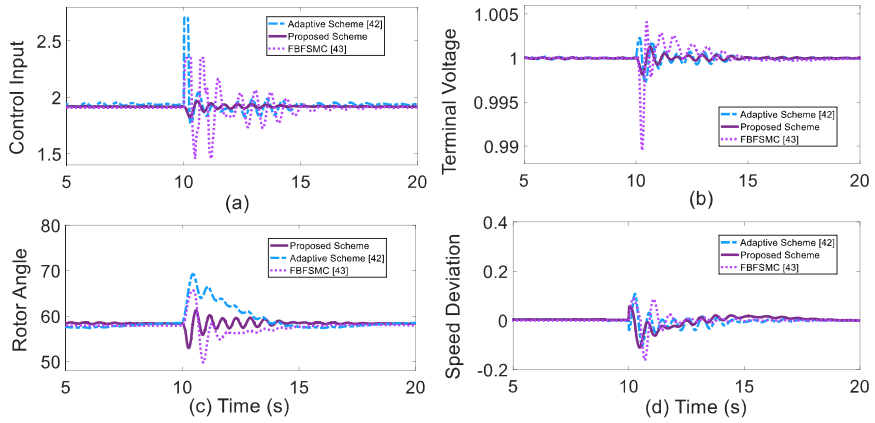


Figure 2.12. Corresponding responses of (a) control input $(pu)$ (b) terminal voltage $(pu)$ (c) rotor angle (d) speed deviation $(pu)$.

This uncertainty causes sudden damping in the synchronous generator states, which may deteriorate the stability regime of the power system. These abrupt uncertainties are compensated by the suppression control CTNO which, along with excitation control (*2.18*) adjusts the tuning gains, as depicted in Figure *2.11*. These gains set the control input damping in a way to adopt the uncertainty in the form of abrupt mechanical power variation. The generator states are stabilized more quickly as compared with the other backstepping schemes, as illustrated in Figure *2.12*. In Figure *2.12*, the control input response, terminal voltage response, rotor angle response, and the speed deviation under case 3 are illustrated.

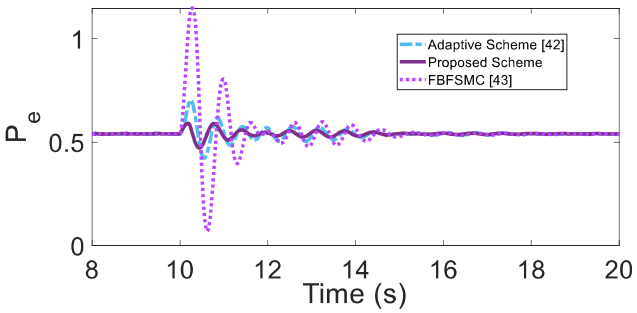


Figure 2.13. Responses to electric power $P_e$ $(pu)$.

The response of electric power under the uncertainty is shown in Figure *2.13*. This uncertainty is when applied in the adaptive scheme [42] and fractional order scheme [43], the higher control variation is observed, and a similar magnitude change is reflected in the corresponding states. The advancement of the proposed scheme is reflected in the obtained results illustrated in Figure *2.12*and Figure *2.13*. Again, it can be observed from case 3 that due to a lack of advancement in the robust scheme and complexity in the control input, the scheme [43] exhibits higher overshoot and sluggish response. Although the operational range in the fractional-order scheme [43] is extended by variation in the fractional coefficient but the computational complexity and control burden is enhanced, which is reflected in the obtained results.

### 2.4.2. Controller resiliency against fault.

*Case 4:* This case study involves the efficacy and resiliency of the proposed control towards the loss of effectiveness. First, we consider the fault modeled by (*2.52*), and this

scenario is simulated with the following fault cases.

(i) A constant fault of $\mathcal{F} = 0.001(pu)$, at $t = 5\ s$.

(ii) A periodic fault of $\mathcal{F} = \{0.001 + 0.0002\sin(20t)\}(pu)$ at $t = 5\ s$.

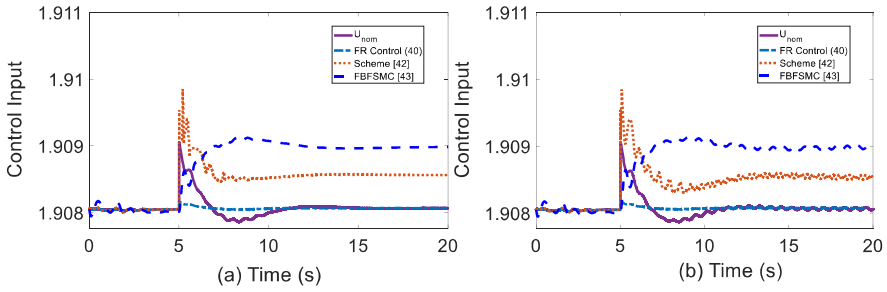


Figure 2.14. Control Input $(pu)$ (a) At constant fault (b) At time-varying fault.

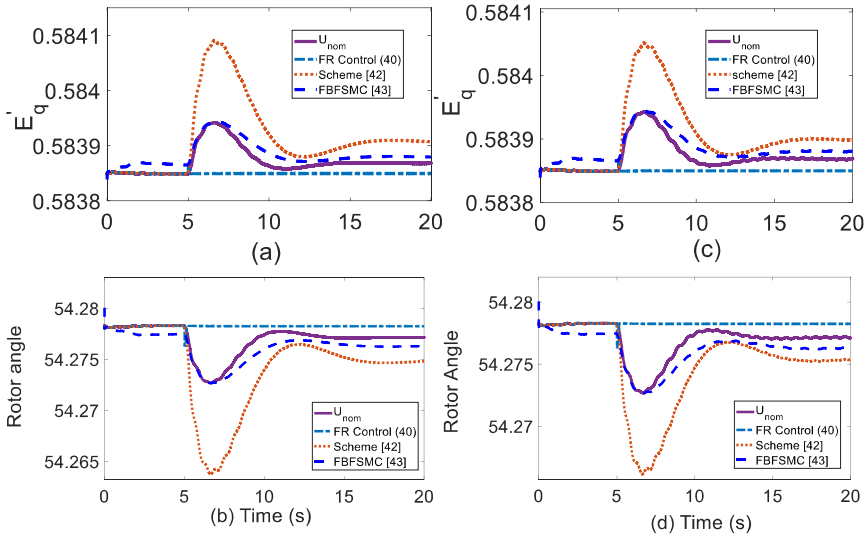


Figure 2.15. Response of power system states under (i) Fault case 1 in $(pu)$ (a) $E'_q$ (b) $\delta$. (ii) Fault case 2 in $(pu)$ (d) $E'_q$ (e) $\delta$.

The results are analyzed for the backstepping schemes presented in [42], [43], nominal control $u_{nom}$ as well as resilient control $(2.53)$ under the subcases (i) and (ii). Faults $\mathcal{F}$ are added at $t = 5\ s$. Corresponding results are illustrated in Figure *2.15*. It can be seen from the results that under backstepping schemes and nominal control $u_{nom}$, machine states, failed to achieve desired equilibrium point, instead states ($E'_q$ and $\delta$) are shifted to another level of equilibrium. Now when resilient control $(2.53)$ is applied for the fault cases (i) & (ii), the correctness of multimachine system states at the original equilibrium point is obtained and faults are rejected. The closed-loop control action corresponding to the fault cases are shown in Figure *2.14*. As seen in Figure *2.14*, due to the

combined control action (*2.18*) and (*2.50*), proposed control required reduced effort compared to backstepping scheme [42] and [43].

## 2.5 Real-Time Verification of the Proposed Scheme

In order to validate the feasibility of the proposed control scheme, the software in loop (SIL) simulation is carried out in real-time digital simulator (RTDS) platform in the existing smart grid lab in the IIT BHU, Varanasi. The smart grid lab has the facility of NovaCor RTDS with four cores available.

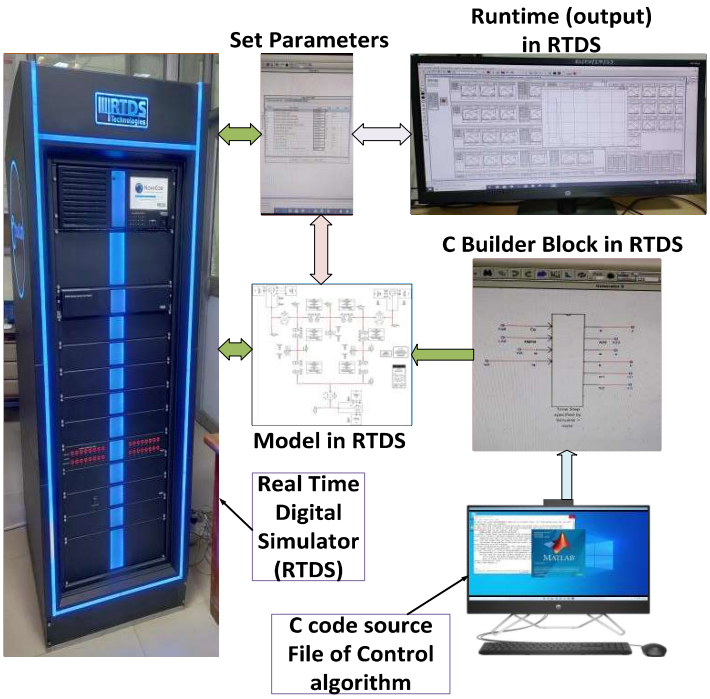


Figure 2.16. Block diagram representation of real-time SIL simulation

The RTDS consists of NovaCor chassis in each rack that is facilitated with POWER8TM processor of IBM's state of the art. It has four powerful cores which can run at a 3.5 GHz frequency. Also, the powerful chassis of NovaCor in RTDS can perform two times faster simulation of a completely loaded PB5 type rack, where the single core can solve hundreds of nodes simultaneously. The real-time simulation verification of the proposed control is done in RTDS environment with the testbed system, as shown in Figure *2.16*. In this experiment, the MATLAB control algorithm function block in Simulink is converted into C code files through the embedded block in Simulink. These C code files are uploaded to the C builder block by designing input-output ports in the component

block of the C builder available in the RTDS tools for the interface with the RTDS model. All variable names with respect to the designed block in the C builder have been carefully named as per the corresponding signal in the RTDS model. After the interface of the Simulink control block with the RTDS via C builder blocks, all parameters are set for the SIL verification. In this way, the SIL testing for the proposed controller is carried out.

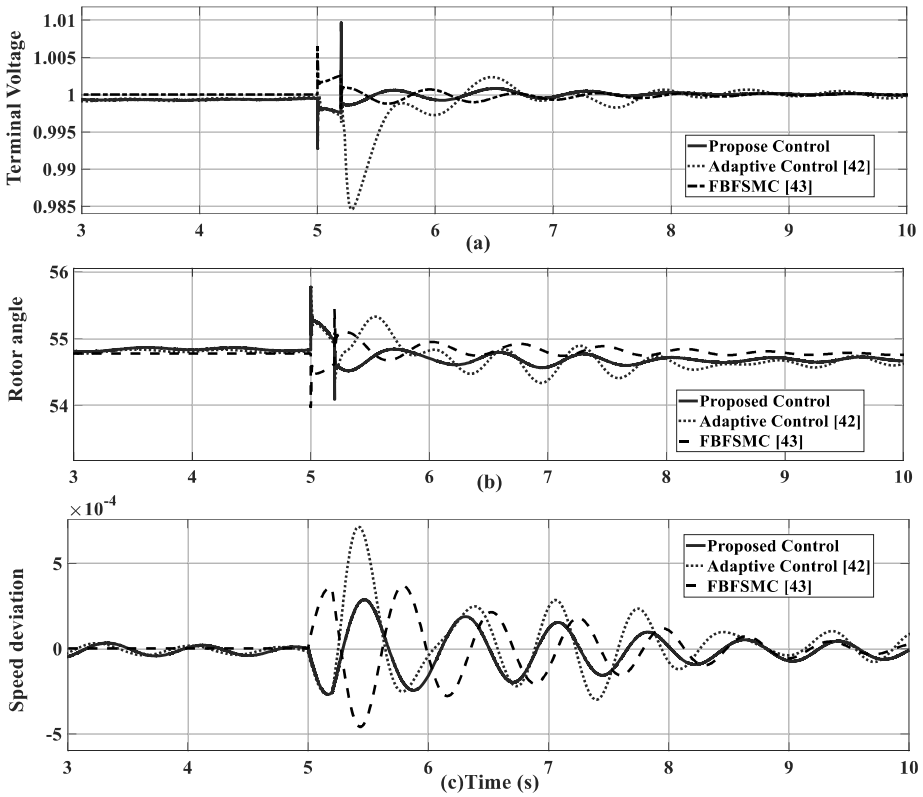


Figure 2.17. Case 5(a) terminal voltage$(pu)$ (b) rotor angle (c) speed deviation $(pu)$.

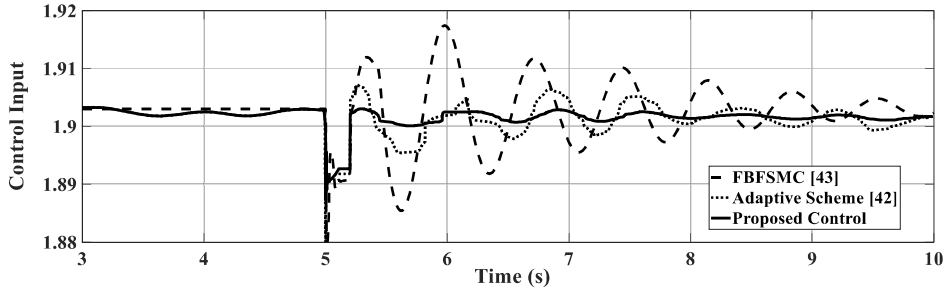


Figure 2.18. Control inputs $(pu)$ of proposed control and adaptive backstepping method [42] and [43].

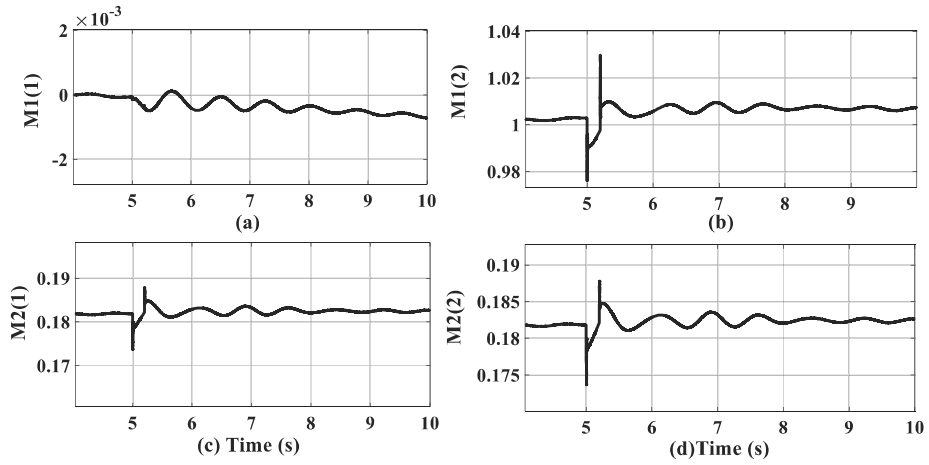


Figure 2.19. Optimal gain parameters (a) M1(1) (b) M1(2) (c) M2(1) (d) M2(2).

*Case 5:* This case is tested in RTDS through the C builder control codes, and the results are analyzed in the runtime RTDS toolbox. In this case transmission line between bus 25 and bus, 26 is temporarily tripped for $0.2\ sec$. This fault is applied at $t = 5\ sec$. The results obtained in this case using the proposed scheme and backstepping schemes [42], [43] (dotted line, dash line, respectively) are shown in Figure *2.17*. The terminal voltage response having fast convergent time and small deviation is reflected in Figure *2.17*(a). Similarly, the rotor angle and speed deviation responses are depicted in Figure *2.17*(b) and (c), respectively.

These responses summarize the fast and strong disturbance rejection capability of the proposed controller compared with the scheme [42] and [43]. The control input response of both schemes is shown in Figure *2.18*. The optimal gain response for case 5 is provided in Figure *2.19*. Here it can be observed that the corresponding variation in optimal gain is reflected with respect to the fluctuation in the power system states due to external perturbation. The improvement in the responses of proposed control scheme is observed due to efficient performance of control input (*2.18*) and CTNO (*2.50*).

## 2.6 Summary

The proposed control with optimally tuned gains eliminates the requirement of extra filters that reduces the computational complexity and improves the power system performance. As the power system nonlinearities are separated in the proposed scheme, it simplifies the control expression and enhances the power system operation regime.

Resilient control along with CTNO compensates for the impact of biased faults in the power system network with mismatched uncertainties, as illustrated in the obtained results. It is also observed from the results that the proposed scheme improves the speed of state convergence with reduced overshoot as compared with the other backstepping methods. The proposed algorithm can be extended for the resiliency towards cyber threats in wide area networks. Also, the multiagent aspect in the proposed control sense can be incorporated in the future for the multimachine power system.